

Research



Cite this article: Lv X, Liu L, Leng J, Liu Y, Cai S. 2019 Delayed electromechanical instability of a viscoelastic dielectric elastomer balloon. *Proc. R. Soc. A* **475**: 20190316.
<http://dx.doi.org/10.1098/rspa.2019.0316>

Received: 22 May 2019

Accepted: 30 July 2019

Subject Areas:

mechanics, mathematical modelling

Keywords:

electromechanical instability, non-convex, viscoelasticity, snap-through, delay

Authors for correspondence:

Yanju Liu

e-mail: yj_liu@hit.edu.cn

Shengqiang Cai

e-mail: shqcai@ucsd.edu

Electronic supplementary material is available online at <https://doi.org/10.6084/m9.figshare.c.4638107>.

Delayed electromechanical instability of a viscoelastic dielectric elastomer balloon

Xiongfei Lv^{1,2}, Liwu Liu¹, Jinsong Leng³, Yanju Liu¹ and Shengqiang Cai²

¹Department of Astronautic Science and Mechanics, Harbin Institute of Technology (HIT), PO Box 301, No. 92 West Dazhi Street, Harbin 150001, People's Republic of China

²Department of Mechanical and Aerospace Engineering, University of California, San Diego, La Jolla, CA 92093, USA

³Centre for Composite Materials and Structures, Science Park of Harbin Institute of Technology (HIT), PO Box 3011, No. 2 Yikuang Street, Harbin 150080, People's Republic of China

SC, 0000-0002-6852-7680

When a dielectric elastomer (DE) balloon is subjected to electromechanical loading, instability may happen. In recent experiments, it has been shown that the instability configuration of a DE balloon under electromechanical loading can be very different from that only subjected to mechanical load. It has also been observed in the experiments that the electromechanical instability phenomena of a DE balloon can be highly time-dependent. In this article, we adopt a nonlinear viscoelastic model for the DE membrane to investigate the time-dependent electromechanical instability of a DE balloon. Using the model, we show that under a constant electromechanical loading, a DE balloon may gradually evolve from a convex shape to a non-convex shape with bulging out in the centre, and compressive hoop stress can also gradually develop the balloon, resulting in wrinkles as observed in the experiments. We have further shown that the snap-through instability phenomenon of the DE balloon also greatly depends on the ramping rate of the applied voltage.

1. Introduction

A dielectric elastomer (DE) membrane can change shape dramatically when subjected to electrical voltage.

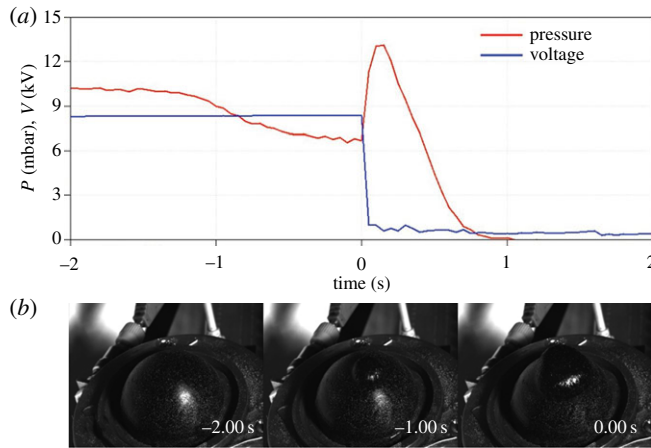


Figure 1. (a) Experimental observation of the shape change of an inflated DE membrane with time under constant electromechanical loading condition [28]. (b) A bulging-out region appears and grows with the increase in time. It is noted that the diameter of the membrane is 4.5 cm. (Online version in colour.)

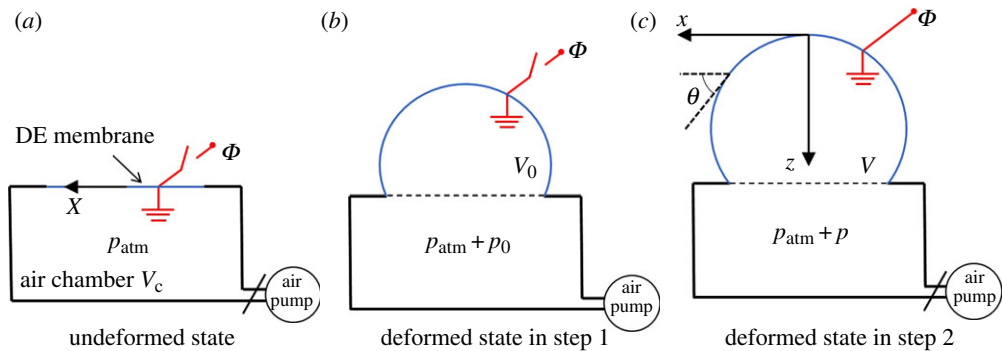


Figure 2. Schematics of the deformation of a DE balloon subjected to electromechanical loading. (a) Undeformed state. (b) First inflation of the DE membrane by an internally applied pressure. (c) Additional deformation of the DE balloon induced by voltage. (Online version in colour.)

Thanks to their fast response, high energy efficiency, great deformability and low cost [1,2], DE membranes have been intensively explored in recent years as soft actuators for the applications of soft robot [3–6] and as strain sensors for numerous biomedical devices [7–9]. In the applications, the interplay of mechanics and electric field in DE can often lead to complex phenomena such as electromechanical pull-in instability [10–12], voltage-induced wrinkling [13,14], creasing and cratering [15–17] and electromechanical bifurcation of a spherical balloon [18,19], to which interpret, detailed modelling is imperative.

Among all the applications of DE membranes, balloon shape has been often adopted. For instance, balloon-like DE structures of different sizes have been designed as tunable lens [20–22], pumps [23–25] and generators [26,27]. In recent experiments [28,29], abnormal bulging out of a DE balloon under electromechanical loading was observed, as shown in figure 1. In the experimental set-up, a DE membrane without prestretch was mounted on the top of an air chamber, which was connected to an air pump through a valve, as shown in the schematics of figure 2. To inflate the DE membrane to a balloon shape, a certain amount of air was first pumped into the air chamber. The valve was then closed, and consequently, the total amount of the air enclosed by the chamber and the DE balloon was fixed. A constant voltage was then applied onto the DE membrane. It was observed that without changing the electromechanical loading condition, the shape of the DE balloon gradually evolved, and a localized bulging-out area formed at the centre of the DE

balloon, as shown in figure 1*b*. Simultaneously, the monitored pressure inside the DE balloon decreased with time (figure 1*a*), indicating the increase in its volume. It is worth mentioning that such bulging-out phenomena have never been reported in a hyperplastic or viscoelastic balloon only subjected to mechanical loading.

To explain the experimental observations described above, theoretical analyses have been conducted [29,30]. In the modelling, a hyperelastic model was adopted for the DE membrane. It has been found that non-convex shapes are indeed possible equilibrium configurations for the DE balloon for a certain range of internal pressure and applied voltage. However, there are still at least two important questions unaddressed in the previous studies. First, it has been shown in both studies [29,30] that the DE balloon with non-convex shape usually has higher free energy than the one with the convex shape for the same pressure and voltage. It remains unclear how the DE balloon with convex shape gradually evolves into a non-convex shape in the experiments with various loading conditions or loading paths. Second, in both previous studies [29,30] the DE membrane was assumed to be a hyperelastic material, and viscoelasticity was ignored. But as has been seen in the experiment [28], even with constant electromechanical loading the shape of the DE balloon can change dramatically with time. In particular, a bulging-out region appears and grows with the increase in time, as shown in figure 1*b*. Such time-dependent behaviour of the DE balloon cannot be explained by the previous model. In addition, although in the experiments [28,29], an extremely low ramping rate of voltage is adopted where viscosity of the DE membrane can be ignored, as pointed out in [28], a higher ramping rate may be more relevant for engineering applications.

Therefore, in this article, we aim to study the time-dependent behaviour of a DE balloon subjected to electromechanical loading, with consideration of the viscoelastic behaviour of the material. The paper is organized as follows. In §2, we briefly summarize the governing equations for a viscoelastic DE membrane inflated by an internal pressure and subjected to an electrical voltage. We then discuss the multiple coexisting equilibrium configurations of the DE balloon in §3. In §§4 and 5, we investigate the effects of viscoelasticity of the DE membrane and the loading dynamics on the evolution of the shape of the DE balloon. All the results are summarized in §6.

2. Governing equations and numerical computation

Figure 2 sketches a circular DE membrane with thickness H and radius R mounted on an air chamber before and after electromechanical loading. The atmosphere pressure is p_{atm} , and the volume of air underneath is V_c . In figure 2*a*, the DE membrane is not subjected to any load. The actuation of the DE membrane can be divided into two steps: first, an initial pressure p_0 is applied to the DE membrane to inflate it into a balloon shape (figure 2*b*). Second, the valve connecting the air pump and the air chamber is closed, and then a voltage Φ is applied onto the DE membrane to induce further deformation with the internal pressure changing to p (figure 2*c*). The volume of the DE balloon is set as V_0 and V after the actuation of steps 1 and 2, respectively.

We first briefly summarize all the governing equations for the system, which have been derived in our previous work [31]. We assume the deformation of the DE membrane is axisymmetric and establish the Cartesian coordinates x - z upon the DE membrane. The x -coordinate is along the horizontal direction and the z -coordinate is along the axis of symmetry. In the undeformed state, each material point occupies a position with the coordinate $(X, 0)$, and all the physical fields in the deformed state can be expressed as a function of X . Considering a material point $(X, 0)$ and its adjacent point $(X + dX, 0)$, they transform into $(x(X), z(X))$ and $(x(X + dX), z(X + dX))$, respectively, in the deformed state, then we have $dx = x(X + dX) - x(X)$ and $dz = z(X + dX) - z(X)$. The distance between the two material points changes from dX to $\lambda_1 dX$, where λ_1 is the stretch in the longitudinal direction. Define $\theta(X)$ as the angle between the tangent of the material point and the horizontal direction in the deformed state, so we have

$$\frac{dx}{dX} = \lambda_1 \cos \theta \quad (2.1)$$

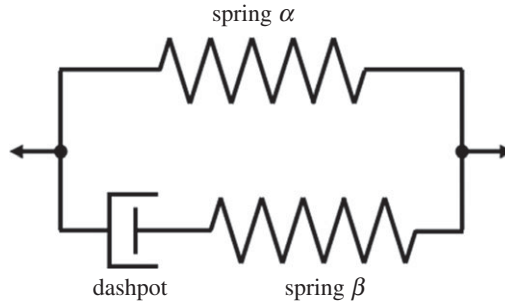


Figure 3. Viscoelastic model of a DE membrane consisting of two springs and one dashpot.

and

$$\frac{dz}{dX} = \lambda_1 \sin \theta. \quad (2.2)$$

Simple geometrical analysis enables us to calculate the longitudinal stretch λ_1 and the latitudinal stretch λ_2 as

$$\lambda_1 = \sqrt{\left(\frac{dx}{dX}\right)^2 + \left(\frac{dz}{dX}\right)^2} \quad (2.3)$$

and

$$\lambda_2 = \frac{x(X)}{X}. \quad (2.4)$$

The force balance equations are

$$\frac{d}{dX}(\sigma_1 h x \cos \theta) + \left(p x - \frac{\sigma_2 h}{\sin \theta} \right) \frac{dz}{dX} = 0 \quad (2.5)$$

and

$$\frac{d}{dX}(\sigma_1 h x \sin \theta) - p x \frac{dx}{dX} = 0, \quad (2.6)$$

where σ_1 and σ_2 are the true stresses in the longitudinal and latitudinal direction, respectively, and $h(X)$ is the thickness of the deformed DE membrane. Simple analysis can show that the inertia of the balloon becomes relevant only when the time scale is shorter than 0.1 s for the system shown in figure 1. Therefore, in equations (2.5) and (2.6) and the following analyses, the inertial effect is ignored.

Following the previous studies, a DE membrane is usually assumed to be incompressible, so

$$h(X) = \frac{H}{\lambda_1 \lambda_2}. \quad (2.7)$$

In order to account for the viscoelasticity of the material, we adopt a specific rheological model [32,33]. As shown in figure 3, a spring α is in parallel with a Maxwell unit (a spring β connected to a dashpot). In the deformed state, the spring α has stretches λ_1 and λ_2 in the two principal directions, and the stretches of the spring β are $\lambda_1 \xi_1^{-1}$ and $\lambda_2 \xi_2^{-1}$, where ξ_1 and ξ_2 are the stretches of the dashpot.

Taking account of the strain stiffening, we write the strain energy of each spring using the Gent model [34]. The total strain energy is the sum of the two springs. In the previous study [28], the authors used the parameter $J_{\text{lim}} = 270$, so we also set $J_{\text{lim}}^\alpha = J_{\text{lim}}^\beta = J_{\text{lim}} = 270$ throughout

this article. With the introduction of $\mu^\alpha + \mu^\beta = \mu$ and $\mu^\alpha / \mu = k$, we can write the total strain energy as

$$W_{\text{Stretch}}(\lambda_1, \lambda_2, \xi_1, \xi_2) = -\frac{k\mu J_{\text{lim}}}{2} \log \left(1 - \frac{\lambda_1^2 + \lambda_2^2 + \lambda_1^{-2}\lambda_2^{-2} - 3}{J_{\text{lim}}} \right) - \frac{(1-k)\mu J_{\text{lim}}}{2} \log \left(1 - \frac{\lambda_1^2 \xi_1^{-2} + \lambda_2^2 \xi_2^{-2} + \lambda_1^{-2}\lambda_2^{-2}\xi_1^2 \xi_2^2 - 3}{J_{\text{lim}}} \right), \quad (2.8)$$

where k determines the viscoelasticity of material. If $k = 1$, the material is purely elastic; while the material behaves like viscous fluid when $k = 0$.

The ideal dielectric elastomer model [35,36] is adopted, as the change of the electrical permittivity ε is negligible with its deformation [37]. The relationship between the electric displacement and electric field is further assumed to be linear, namely

$$D = \varepsilon E. \quad (2.9)$$

The constitutive model of an incompressible, ideal dielectric elastomer membrane gives the relation between true stresses and stretches as [36,38]

$$\sigma_1 + \varepsilon E^2 = \frac{k\mu(\lambda_1^2 - \lambda_1^{-2}\lambda_2^{-2})}{1 - (\lambda_1^2 + \lambda_2^2 + \lambda_1^{-2}\lambda_2^{-2} - 3)/J_{\text{lim}}} + \frac{(1-k)\mu(\lambda_1^2 \xi_1^{-2} - \lambda_1^{-2}\xi_1^2 \lambda_2^{-2}\xi_2^2)}{1 - (\lambda_1^2 \xi_1^{-2} + \lambda_2^2 \xi_2^{-2} + \lambda_1^{-2}\xi_1^2 \lambda_2^{-2}\xi_2^2 - 3)/J_{\text{lim}}} \quad (2.10)$$

and

$$\sigma_2 + \varepsilon E^2 = \frac{k\mu(\lambda_2^2 - \lambda_1^{-2}\lambda_2^{-2})}{1 - (\lambda_1^2 + \lambda_2^2 + \lambda_1^{-2}\lambda_2^{-2} - 3)/J_{\text{lim}}} + \frac{(1-k)\mu(\lambda_2^2 \xi_2^{-2} - \lambda_1^{-2}\xi_1^2 \lambda_2^{-2}\xi_2^2)}{1 - (\lambda_1^2 \xi_1^{-2} + \lambda_2^2 \xi_2^{-2} + \lambda_1^{-2}\xi_1^2 \lambda_2^{-2}\xi_2^2 - 3)/J_{\text{lim}}}. \quad (2.11)$$

In the Maxwell unit, the dashpot is subjected to the same true stresses as the spring β . The true strain rates in the dashpot are given by

$$\frac{d\xi_1}{\xi_1 dt} = \frac{1}{3\eta} \left(\begin{array}{l} \frac{(1-k)\mu(\lambda_1^2 \xi_1^{-2} - \lambda_1^{-2}\xi_1^2 \lambda_2^{-2}\xi_2^2)}{1 - (\lambda_1^2 \xi_1^{-2} + \lambda_2^2 \xi_2^{-2} + \lambda_1^{-2}\xi_1^2 \lambda_2^{-2}\xi_2^2 - 3)/J_{\text{lim}}} \\ - \frac{(1-k)\mu(\lambda_2^2 \xi_2^{-2} - \lambda_1^{-2}\xi_1^2 \lambda_2^{-2}\xi_2^2)/2}{1 - (\lambda_1^2 \xi_1^{-2} + \lambda_2^2 \xi_2^{-2} + \lambda_1^{-2}\xi_1^2 \lambda_2^{-2}\xi_2^2 - 3)/J_{\text{lim}}} \end{array} \right), \quad (2.12)$$

and

$$\frac{d\xi_2}{\xi_2 dt} = \frac{1}{3\eta} \left(\begin{array}{l} \frac{(1-k)\mu(\lambda_2^2 \xi_2^{-2} - \lambda_1^{-2}\xi_1^2 \lambda_2^{-2}\xi_2^2)}{1 - (\lambda_1^2 \xi_1^{-2} + \lambda_2^2 \xi_2^{-2} + \lambda_1^{-2}\xi_1^2 \lambda_2^{-2}\xi_2^2 - 3)/J_{\text{lim}}} \\ - \frac{(1-k)\mu(\lambda_1^2 \xi_1^{-2} - \lambda_1^{-2}\xi_1^2 \lambda_2^{-2}\xi_2^2)/2}{1 - (\lambda_1^2 \xi_1^{-2} + \lambda_2^2 \xi_2^{-2} + \lambda_1^{-2}\xi_1^2 \lambda_2^{-2}\xi_2^2 - 3)/J_{\text{lim}}} \end{array} \right) \quad (2.13)$$

where η is the viscosity of the dashpot. The relaxation time is determined by the viscosity of the dashpot and the elastic modulus of the spring β

$$t_v = \frac{\eta}{(1-k)\mu}. \quad (2.14)$$

Previous experiment tests have shown that the spectrum of the relaxation time of the VHB elastomer ranges from subseconds to tens of minutes [39–41]. However, to simplify the problem, we assume a single relaxation time scale in the following analyses.

In order to solve equations (2.1)–(2.14), we rewrite the force balance equations (2.5) and (2.6) as

$$\frac{d\theta}{dX} = -\frac{\sigma_2\lambda_1 \sin \theta}{\sigma_1\lambda_2 X} + \frac{p\lambda_1^2\lambda_2}{\sigma_1 H} \quad (2.15)$$

and

$$\frac{d\lambda_1}{dX} = \left[X \frac{\partial}{\partial \lambda_1} \left(\frac{\sigma_1}{\lambda_1} \right) \right]^{-1} \left[\frac{\sigma_2}{\lambda_2} \cos \theta - \frac{\sigma_1}{\lambda_1} - \frac{\partial}{\partial \lambda_2} \left(\frac{\sigma_1}{\lambda_1} \right) (\lambda_1 \cos \theta - \lambda_2) \right]. \quad (2.16)$$

Equations (2.15) and (2.16) together with (2.1) and (2.2) constitute the first set of differential equations, determining the deformation field of the DE membrane at any time t . The boundary conditions are

$$x(0, t) = 0, \quad z(0, t) = 0, \quad \theta(0, t) = 0, \quad x(R, t) = R. \quad (2.17)$$

Equations (2.12) and (2.13) provide the second set of differential equations with unknowns $\xi_1(X, t)$ and $\xi_2(X, t)$. In all the following computations, we assume the pre-deformation of the DE membrane before its shape evolution is instantaneous, so we have the initial conditions for the dashpot as

$$\xi_1(X, 0) = 1, \quad \xi_2(X, 0) = 1. \quad (2.18)$$

In the computation, we use the following dimensionless quantities: x -coordinate x/R , z -coordinate z/R , volume V/R^3 , pressure $pR/\mu H$, voltage $\Phi/H\sqrt{\mu/\varepsilon}$, time t/t_v and the modulus ratio k , which is fixed as 0.5 in the current work. At time $t=0$, the dashpot has no deformation. If $pR/\mu H$ and $\Phi/H\sqrt{\mu/\varepsilon}$ are given, the first set of differential equations can be solved by using the shooting method. Once $\lambda_1(X, 0)$ and $\lambda_2(X, 0)$ are known, with an appropriate time increment Δt , the stretches of the dashpot $\xi_1(X, \Delta t)$ and $\xi_2(X, \Delta t)$ can be solved from the second set of differential equations. With knowing the loading parameters $pR/\mu H$ and $\Phi/H\sqrt{\mu/\varepsilon}$, we can further update all the physical fields by using the first set of differential equations again. It is worth noting that at time $t = \Delta t$, if we keep the total amount of air as a constant, the pressure will drop with the increase in the volume, so we need to find a new pressure p at this moment that satisfies the ideal gas law

$$NKT = (p + p_{\text{atm}})(V + V_c) = (p_0 + p_{\text{atm}})(V_0 + V_c), \quad (2.19)$$

where the normalized atmosphere pressure $p_{\text{atm}}R/\mu H = 100$ will be used throughout our paper. Repeating this procedure by continuously increasing the time, all the physical fields can be determined step by step.

3. Equilibrium states and loading paths

We first compute the possible equilibrium states of the DE balloon by ignoring the viscous effects of the material. When k is set to be one in equations (2.8), (2.10) and (2.11), we obtain the governing equations for a hyperelastic DE balloon. The pressure–volume relationship for the DE balloon for several different voltages is plotted in figure 4. When the voltage is low, the pressure–volume curves have N -like shapes. When the applied voltage is higher than a critical value (higher than 0.145), the shapes of the curves become more complex, which have been discussed in detail in previous studies [29,30].

It is noted that in previous studies [29,30], five equilibrium configurations of the DE balloon can be found in a certain range of internal pressure and applied voltage. With more detailed calculations, we further find that in the current study that seven equilibrium configurations of the DE balloon can exist for a certain range of pressure and voltage (e.g. $\Phi/H\sqrt{\mu/\varepsilon} = 0.17$ and $1.468 < pR/\mu H < 1.478$). For the seven equilibrium configurations, four of them (A, C, F, G) have convex shapes and three (B, D, E) have non-convex shapes, as shown in figure 5.

Although multiple equilibrium states can exist at the same pressure and voltage, it is difficult to obtain all those equilibrium states in the experiment. For instance, if the applied voltage is

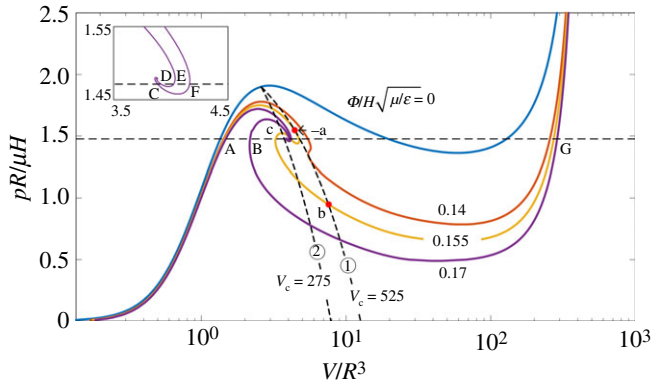


Figure 4. Pressure–volume curves of a DE balloon at several different voltages. Dashed curve 1 is for $V_c/R^3 = 525$, and dashed curve 2 is for $V_c/R^3 = 275$. (Online version in colour.)

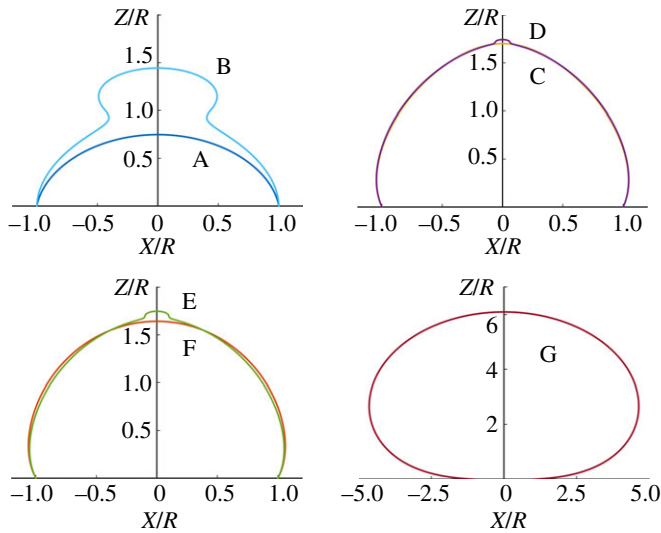


Figure 5. Seven distinct configurations at pressure $pR/\mu H = 1.47$ and voltage $\Phi/H\sqrt{\mu/\varepsilon} = 0.17$. (Online version in colour.)

fixed, with the pressure-control mode, the DE balloon will snap from a state of small volume to a state of large volume when the pressure reaches the first peak of the pressure–volume curve of the DE balloon. All the configurations between the two states cannot be achieved in experiment.

In the experiments described previously [28,29], the DE membrane is first inflated to a balloon shape. Subsequently, the valve is closed to fix the total amount of air enclosed by the DE balloon and the chamber. Then a voltage is applied onto the balloon. In this case, with the increase in the balloon volume induced by the voltage, the internal pressure drops, which can stabilize some of the equilibrium states of the DE balloon located in the descending paths in the pressure–volume curves in figure 4. For two different representative volumes of the air chamber $V_c/R^3 = 525$ and 275 and with the initial pressure $p_0R/\mu H = 1.9$, the relationships between the volume of the DE balloon and the internal pressure given by equation (2.19) are represented by the two dashed curves in figure 4 for the fixed total amount of enclosed air. Therefore, with the increase in the voltage and valve being closed, the state of the balloon moves along one of the dashed curves (depending on the volume of the air chamber).

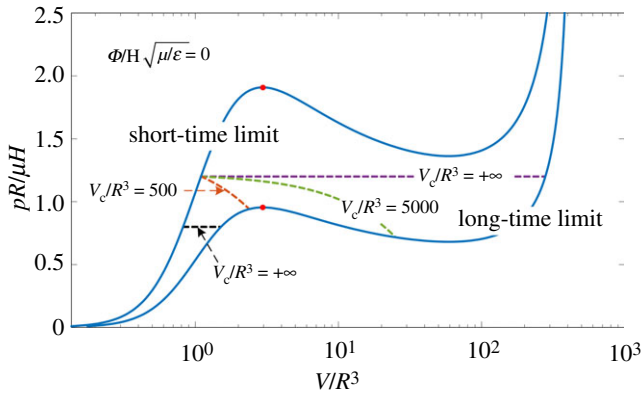


Figure 6. Short-time and long-time limit of pressure–volume curves of a viscoelastic DE balloon only subjected to internal pressure. The horizontal dashed lines represent the evolution of the DE balloon with a fixed pressure. The dashed curves represent the evolution of the DE balloon with a fixed amount of enclosed air with two different air chamber volumes, $V_c/R^3 = 500$ and 5000. (Online version in colour.)

4. Evolution of the shape of the dielectric elastomer balloon subjected to a constant voltage and with a fixed amount of enclosed air

In this section, we study the effects of the viscoelasticity of the DE material on the shape evolution of the DE balloon with a constant electromechanical loading. To understand the phenomena described in the experiment and as shown in figure 1, we assume the DE balloon at time $t = 0$ is first inflated by an internal pressure and then subjected to a voltage instantaneously. After that ($t > 0$), the applied voltage is maintained unchanged and the valve connecting the air pump and the air chamber is closed, namely, the total amount of air enclosed by the chamber and the DE balloon is fixed. The change in the shape of the DE balloon with time can be computed.

To better understand the phenomenon, we first study the case with no applied voltage. In the short-time limit ($t = 0$), the dashpot in the model (as shown in figure 3) has no deformation and the stresses are taken by the two springs, so we have $\xi_1 = \xi_2 = 1$. In the long-time limit ($t \rightarrow +\infty$), the stresses on the dashpot are completely relaxed, and stresses are only taken by the spring α , so we have $\lambda_1 = \xi_1$ and $\lambda_2 = \xi_2$. We plot the pressure–volume relationship for the DE balloon for both short-time limit and long-time limit in figure 6.

We first consider the case with a constant internal pressure applied to the DE balloon, which is equivalent to the case with an air chamber of infinitely large volume. If the pressure is low (e.g. the pressure is below the first peak value of the pressure–volume curve for the long-time limit), the volume of the DE balloon increases continuously from the short-time limit to the long-time limit (figures 6 and 7a). However, if the applied pressure is high (the pressure is below the peak of the pressure–volume curve for the short-time limit but above the peak of the pressure–volume curve for the long-time limit), the volume of the DE balloon increases continuously first and then snaps to a large value, as shown in figures 6 and 7a.

We can predict similar phenomena for the case of fixing the total amount of air enclosed by the air chamber together with the DE balloon. Since the total amount of air is fixed, the pressure applied to the DE balloon and its volume have to be related by the ideal gas law (equation (2.19)). With two different volumes of the air chamber ($V_c/R^3 = 500$ and 5000), equation (2.19) can be represented by two different dashed curves, as shown in figure 6. We assume that the DE balloon is first inflated instantly to a volume with the initial pressure $p_0R/\mu H = 1.2$. If the volume of the air chamber is small ($V_c/R^3 = 500$), the volume of the DE balloon gradually increases due to the stress relaxation in the DE membrane, finally reaching an equilibrium state, as shown in figure 7b. If the volume of the air chamber is large ($V_c/R^3 = 5000$), the DE balloon can snap from a state with

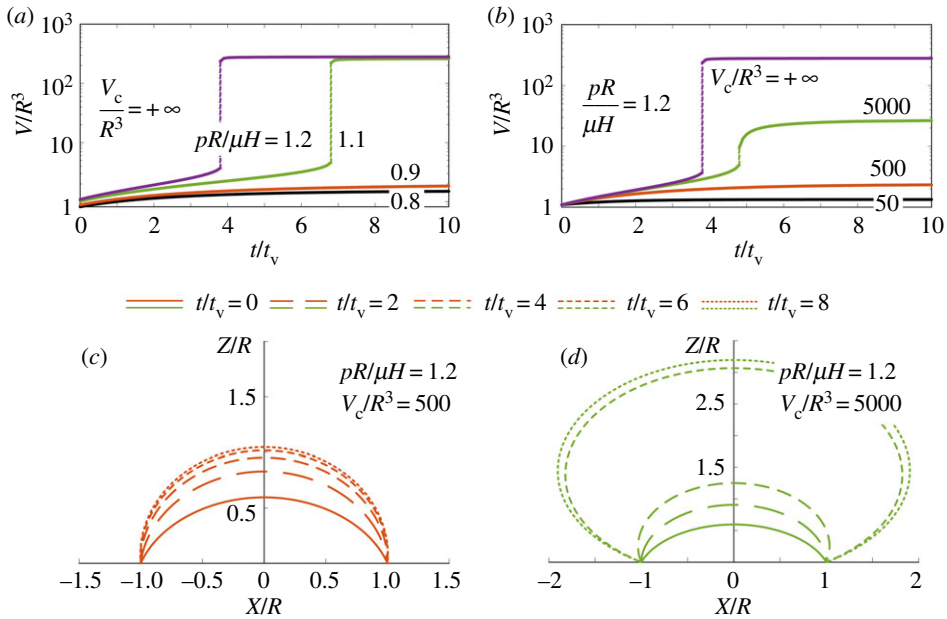


Figure 7. (a) Volume of the DE balloon changes with time with different internal pressures. (b) Volume of the DE balloon changes with time with a fixed amount of enclosed air for four different volumes of the air chamber. (c) Shape of the DE balloon at several different time points with the air chamber volume $V_c/R^3 = 500$. (d) Shape of the DE balloon at several different time points with the air chamber volume $V_c/R^3 = 5000$. (Online version in colour.)

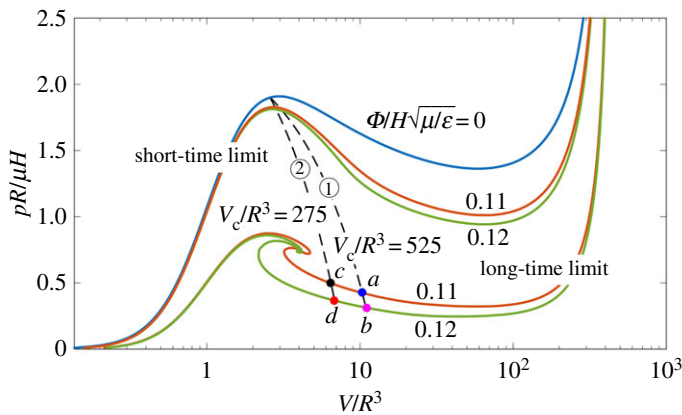


Figure 8. Short-time and long-time limit of pressure–volume curves with two different voltages $\Phi/H\sqrt{\mu/\varepsilon} = 0.11$ and 0.12 . With the fixed amount of enclosed air, the DE balloon can change its volume along different paths, represented by the two dashed curves, depending on the air chamber volumes, $V_c/R^3 = 525$ and 275 . (Online version in colour.)

small volume to a state with large volume, as shown in figures 6 and 7*b*. Detailed computations provide a complete process of the evolution of the shape of the DE balloon, as shown in figure 7*c,d*. It is noted that, in the computation, we ignore the inertia of the DE balloon. In other words, we assume the discontinuous snap through of the DE balloon takes no time.

Next, we study the case with applied voltage. Similar to figure 6, figure 8 plots the short-time and long-time limit of pressure–volume curves with two different voltages $\Phi/H\sqrt{\mu/\varepsilon} = 0.11$ and 0.12 . The change of the volume of the DE balloon with time for two different level of voltages and two fixed different volumes of air chamber $V_c/R^3 = 525$ and 275 are shown in figure 9*a,d*.

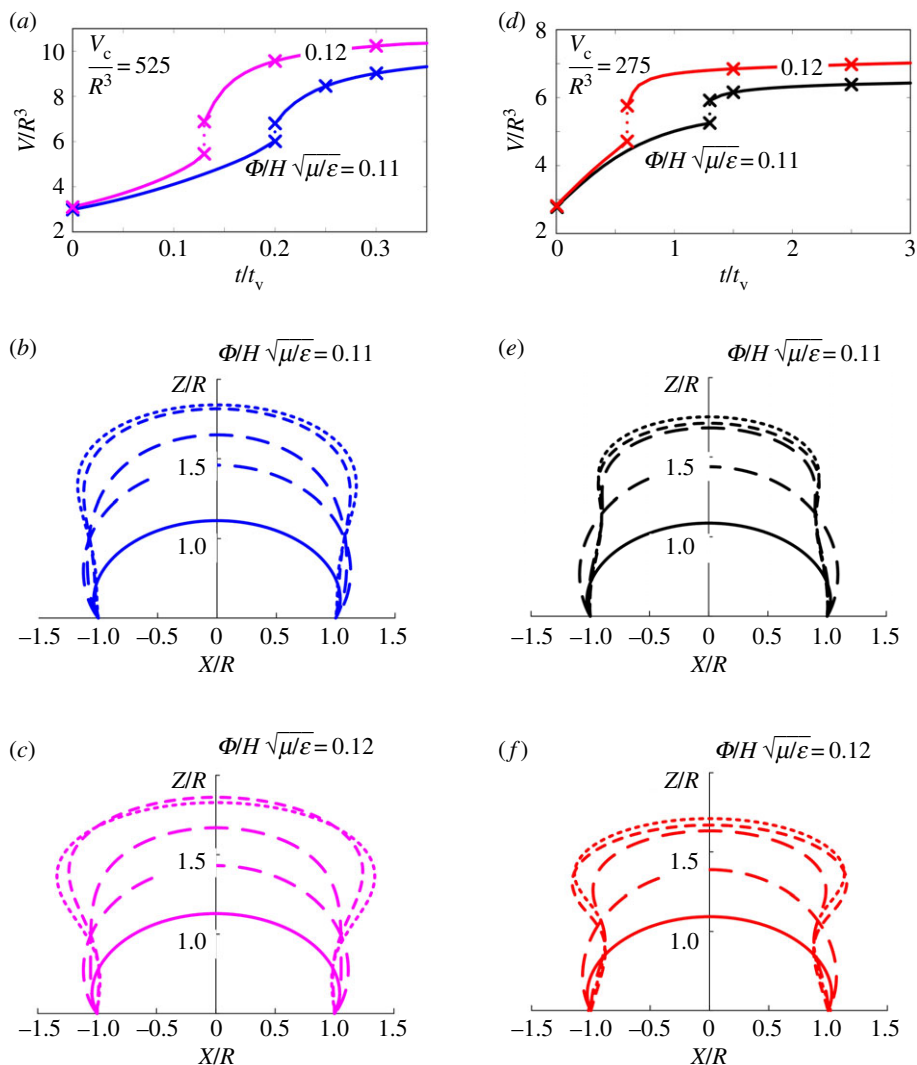


Figure 9. Volume–time curves of the DE balloon and some typical configurations of the DE balloon at the time points marked on the volume–time curves for two different air chamber volumes, $V_c/R^3 = 525$ (a–c) and 275 (d–f). (Online version in colour.)

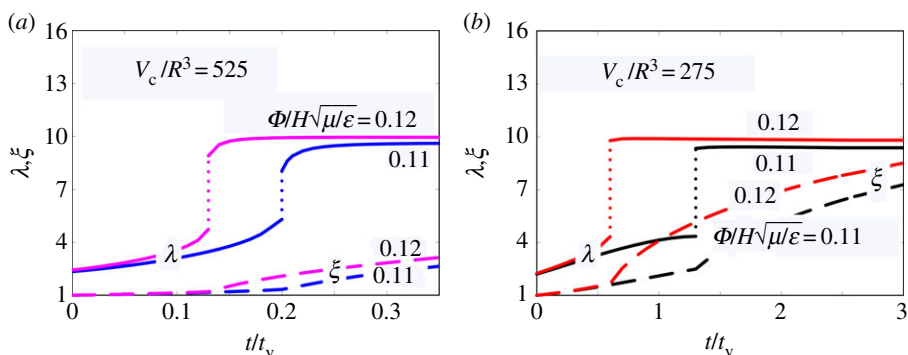


Figure 10. (a, b) Stretch evolution of spring α (solid curves) and dashpot (dashed curves) at the centre of the DE balloon for two different air chamber volumes, $V_c/R^3 = 525$ and 275 . (Online version in colour.)

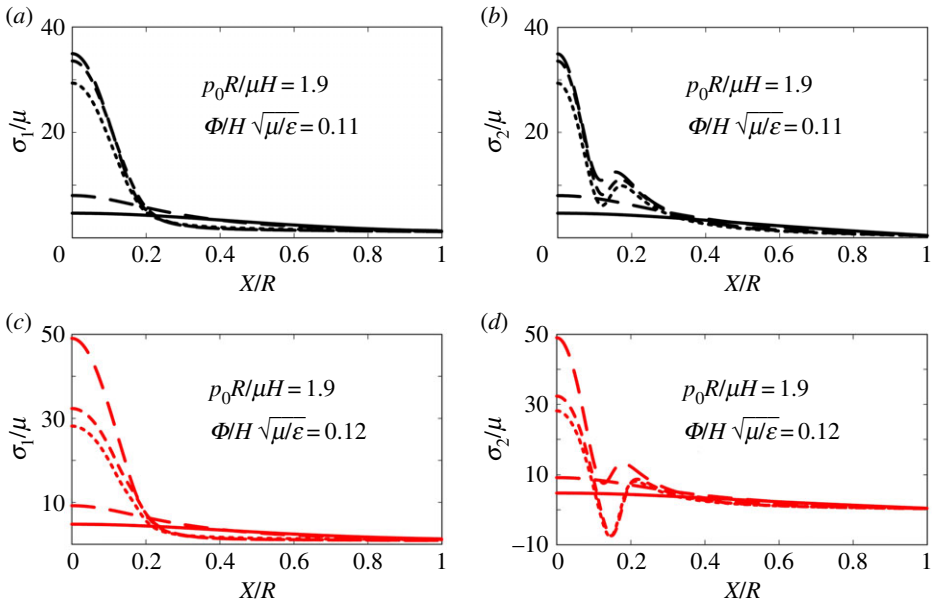


Figure 11. Stress distributions in the DE balloon under the voltage $\Phi/H\sqrt{\mu/\epsilon} = 0.11$ (a,b) and 0.12 (c,d) at the time points marked on the volume–time curves in figure 9d. (Online version in colour.)

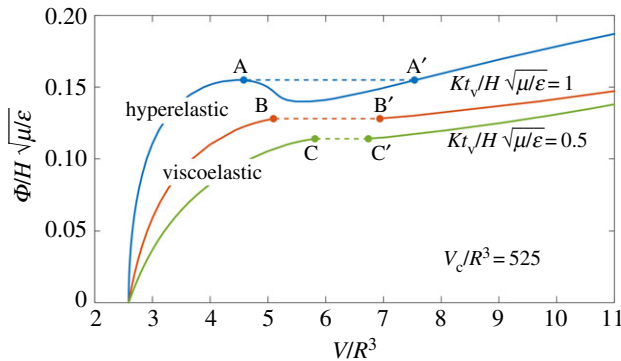


Figure 12. The relationship between the voltage and the volume of the DE balloon for a fixed amount of enclosed air with the air chamber volume $V_c/R^3 = 525$, for two different voltage ramping rates, as well as the case of neglecting material viscosity. (Online version in colour.)

Figure 9b,c and e,f plots the configurations of balloons at the points marked on the volume–time curves in figure 9a,d, respectively. It can be seen that the DE balloon can evolve from an initial configuration with convex shape to a configuration with non-convex shape, which is very similar to the formation of a bulging-out area in an inflated DE membrane with fixed electromechanical loads, as reported in [28] and shown in figure 1.

We further plot the evolution of the stretch at the centre of the DE balloon in figure 10 and the stress distribution in the DE balloon at several different times in figure 11. As we can see, the stretch may increase dramatically with the increase in time, which can lead to the failure of the DE balloon as seen in the experiment [28,29]. With the increase in time, the hoop stress in the DE balloon can also change from tensile to compressive, as shown in figure 11d. The compressive stress can cause wrinkles in the DE balloon, which has also been seen in the experiments [28,29,42].

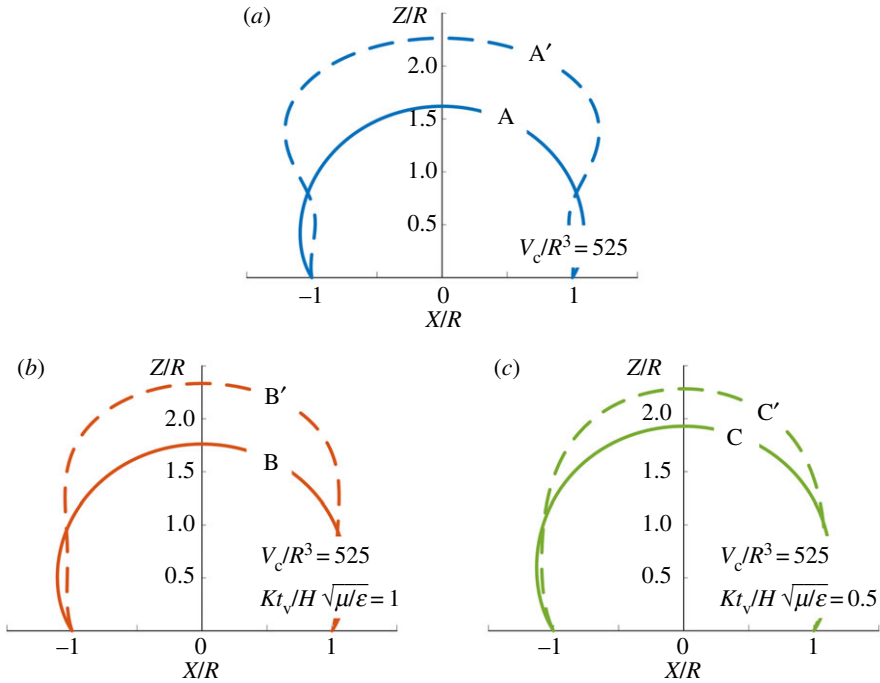


Figure 13. (a–c) The configurations of the DE balloon before (solid curves) and after (dashed curves) snap through for the three cases shown in figure 12. (Online version in colour.)

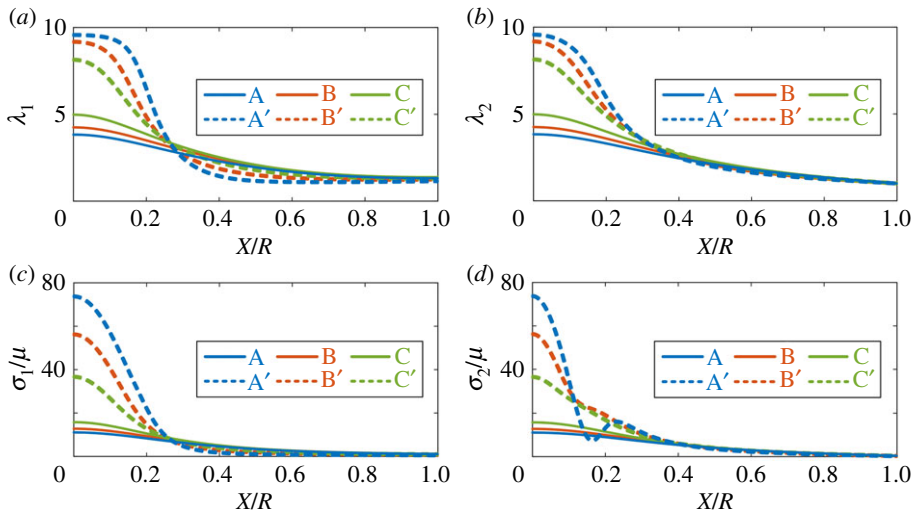


Figure 14. (a–d) Stretch and stress distributions in the DE balloon with the configurations shown in figure 13. Solid and dashed curves are for the configurations before and after snap through, respectively. (Online version in colour.)

As shown in the experiment [28] as well as figure 1, with a fixed voltage, the inflated DE membrane evolves from a convex shape to a partially concave shape within several seconds, which is consistent with the predictions shown in figure 9 when considering that the relaxation time scale (t_V) of VHB membrane is around several seconds [39–41]. In addition, with the results from figure 10, we can predict that the true electric field on the centre of the DE membrane can jump from the value lower than its electrical breakdown field to the value above the electrical

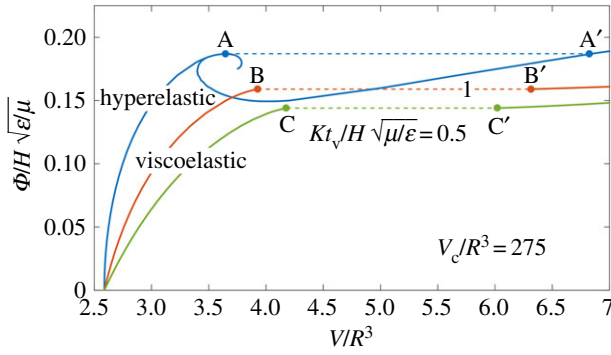


Figure 15. The relationship between the voltage and the volume of the DE balloon for a fixed amount of enclosed air with the air chamber volume $V_c/R^3 = 275$, for two different voltage ramping rates, as well as the case of neglecting material viscosity. (Online version in colour.)

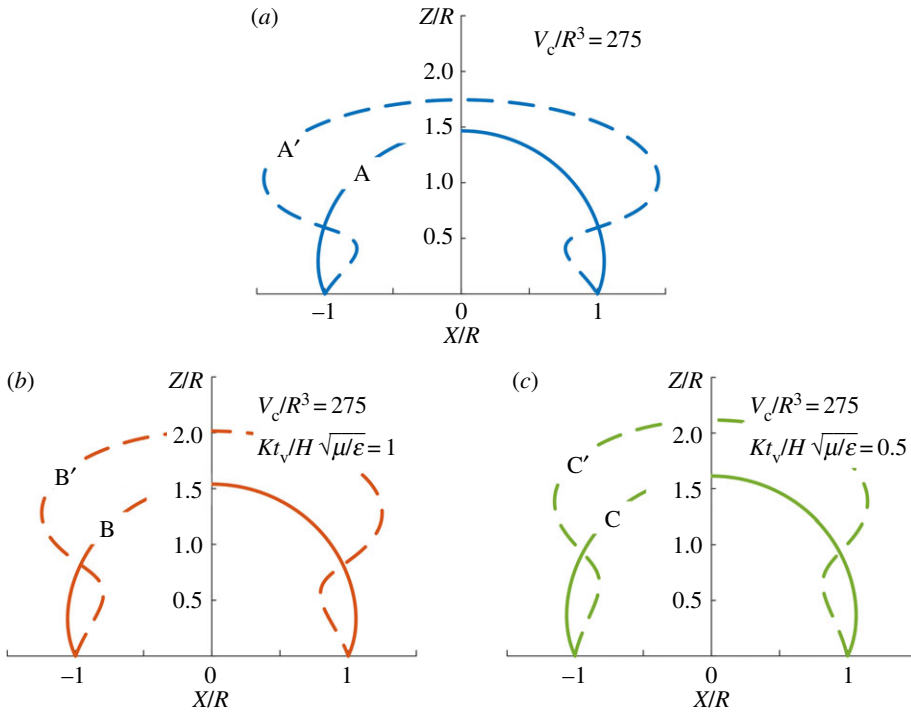


Figure 16. (a–c) The configurations of the DE balloon before (solid curves) and after (dashed curves) snap through for the three cases shown in figure 15. (Online version in colour.)

breakdown field, which is also consistent with the experimental observation that the formation of the bulging-out area often leads to the final failure of the DE membrane.

5. Effects of ramping rate of voltage on the shape of the dielectric elastomer balloon

In this section, we investigate the effects of the ramping rate of the applied voltage on the evolution of the shape of the DE balloon. We assume that the DE balloon is first instantaneously inflated to a volume with the initial pressure $p_0R/\mu H = 1.9$ at $t = 0$. The air enclosed in the

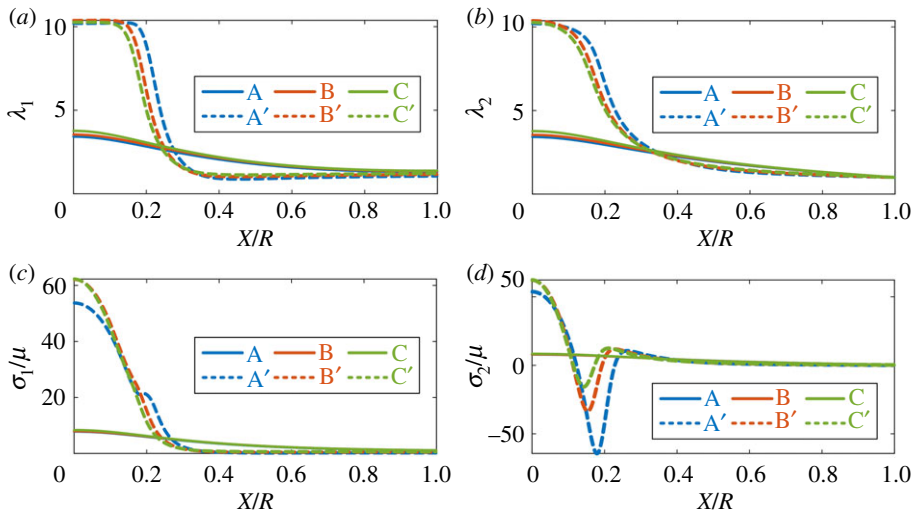


Figure 17. (a–d) Stretch and stress distributions in the DE balloon of the configurations shown in figure 16. Solid and dashed curves are for the configurations before and after snap through, respectively. (Online version in colour.)

system is then fixed. Finally, a voltage is applied onto the DE balloon with a constant ramping rate, namely $\Phi = Kt$ with two different dimensionless ramping rates $Kt_v/H\sqrt{\mu/\varepsilon} = 1$ and 0.5 , respectively; the relationship between the volume of the DE balloon and the voltage is plotted in figure 12 with the volume of the air chamber $V_c/R^3 = 525$, where significant rate-dependence is demonstrated.

For the three different cases in figure 12, snap-through phenomena of the DE balloon can be predicted when the applied voltage reaches a critical value. With the decrease in the ramping rate, lower voltage is needed to trigger the snap-through instability of the DE balloon. This is because with the decrease in the ramping rate of voltage, the effective modulus of the viscoelastic DE membrane also decreases. The shape of the DE balloon for the three cases before and after the snap through is plotted in figure 13.

Figure 14 shows the corresponding stretch and stress distributions of the DE balloon with the configurations shown in figure 13. The solid and dashed curves represent the distributions before and after snap through, respectively. It is shown that after snap through, the stretch and stress at the centre of the DE balloon change most dramatically.

Figure 15 plots the the relationship between the volume of the DE balloon and the voltage with a smaller air chamber $V_c/R^3 = 275$, for two different voltage ramping rates $Kt_v/H\sqrt{\mu/\varepsilon} = 1$ and 0.5 . Comparing it to figure 12, we can see the critical voltage to trigger snap through is higher with the same voltage ramping rate. The shape of the DE balloon before and after the snap through is plotted in figure 16. Figure 17 plots the stretch and stress distributions of the configurations in figure 16. After the snap through, compressive hoop stress may be induced, as shown in figure 17d, resulting in wrinkles on the DE balloon.

6. Conclusion

In this work, we have studied the time-dependent phenomenon of a DE balloon subjected to electromechanical loading. In the model, viscoelasticity of the DE membrane is taken into account. Our computational results show that with a constant electromechanical loading, a DE balloon with convex shape can gradually evolve into a non-convex shape, accompanied by snap-through phenomenon, and also possibly the development of compressive hoop stress. According to our knowledge, such time-dependent shape transition (from convex to non-convex) of a balloon has never been predicted in the previous theoretical or computation studies of dielectric elastomers.

Moreover, we have also studied the rate-dependent behaviour of an inflated DE balloon subjected to voltage of various ramping rates. We found that the critical voltage for inducing the snap-through instability of the DE balloon decreases with the decrease in the ramping rate of the applied voltage or the increase in the volume of the air chamber.

Data accessibility. The code used to solve the deformation field of dielectric elastomer balloon subject to a fixed amount of air and fixed voltage is provided as electronic supplementary material.

Authors' contributions. X.L. derived, coded and solved the equations for the problem. L.L. participated in discussing the problem in computing. Y.L. and J.L. guided the overall idea of the paper. S.C. proposed the initial idea for the paper, arranged the paper's structure and revised the paper's language. All authors gave final approval for publication and agree to be held accountable for the work performed therein.

Competing interests. We declare we have no competing interests.

Funding. S.C. acknowledges the support from the Office of Naval Research with grant no. N000141712062. J.L. acknowledges the support from the National Natural Science Foundation of China (grant no. 11632005). L.L. acknowledges the support from the National Natural Science Foundation of China (grant no. 11772109). X.L. acknowledges the support from the Foreign Short-term Visiting Program for Doctoral Students at HIT.

Acknowledgements. The authors thank the anonymous reviewers whose suggestions helped improve the quality of the paper.

References

1. Pelrine R. 2000 High-speed electrically actuated elastomers with strain greater than 100%. *Science* **287**, 836–839. (doi:10.1126/science.287.5454.836)
2. Carpi F, Bauer S, De Rossi D. 2010 Stretching dielectric elastomer performance. *Science* **330**, 1759–1761. (doi:10.1126/science.1194773)
3. Shintake J, Rosset S, Schubert B, Floreano D, Shea H. 2015 Versatile soft grippers with intrinsic electroadhesion based on multifunctional polymer actuators. *Adv. Mater.* **28**, 231–238. (doi:10.1002/adma.201504264)
4. Li T *et al.* 2017 Fast-moving soft electronic fish. *Sci. Adv.* **3**, e1602045. (doi:10.1126/sciadv.1602045)
5. Christianson C, Goldberg NN, Deheyn DD, Cai S, Tolley MT. 2018 Translucent soft robots driven by frameless fluid electrode dielectric elastomer actuators. *Sci. Robot.* **3**, eaat1893. (doi:10.1126/scirobotics.aat1893)
6. Li J, Liu L, Liu Y, Leng J. 2019 Dielectric elastomer spring-roll bending actuators: applications in soft robotics and design. *Soft Robot.* **6**, 69–81. (doi:10.1089/soro.2018.0037)
7. Lee B-Y, Kim J, Kim H, Kim C, Lee S-D. 2016 Low-cost flexible pressure sensor based on dielectric elastomer film with micro-pores. *Sensor. Actuat. A Phys.* **240**, 103–109. (doi:10.1016/j.sna.2016.01.037)
8. Zhang H, Wang MY, Li J, Zhu J. 2016 A soft compressive sensor using dielectric elastomers. *Smart Mater. Struct.* **25**, 35045. (doi:10.1088/0964-1726/25/3/035045)
9. Huang B, Li M, Mei T, McCoul D, Qin S, Zhao Z, Zhao J. 2017 Wearable stretch sensors for motion measurement of the wrist joint based on dielectric elastomers. *Sensors (Basel)* **17**, 2708. (doi:10.3390/s17122708)
10. Plante J-S, Dubowsky S. 2006 Large-scale failure modes of dielectric elastomer actuators. *Int. J. Solids Struct.* **43**, 7727–7751. (doi:10.1016/j.ijsolstr.2006.03.026)
11. Zhao X, Suo Z. 2007 Method to analyze electromechanical stability of dielectric elastomers. *Appl. Phys. Lett.* **91**, 61921. (doi:10.1063/1.2768641)
12. Leng J, Liu L, Liu Y, Yu K, Sun S. 2009 Electromechanical stability of dielectric elastomer. *Appl. Phys. Lett.* **94**, 211901. (doi:10.1063/1.3138153)
13. Zhu J, Kolloosche M, Lu T, Kofod G, Suo Z. 2012 Two types of transitions to wrinkles in dielectric elastomers. *Soft Matter* **8**, 8840–8846. (doi:10.1039/c2sm26034d)
14. Kolloosche M, Kofod G, Suo Z, Zhu J. 2015 Temporal evolution and instability in a viscoelastic dielectric elastomer. *J. Mech. Phys. Solids* **76**, 47–64. (doi:10.1016/j.jmps.2014.11.013)
15. Wang Q, Tahir M, Zhang L, Zhao X. 2011 Electro-creasing instability in deformed polymers: experiment and theory. *Soft Matter* **7**, 6583. (doi:10.1039/c1sm05645j)
16. Wang Q, Zhang L, Zhao X. 2011 Creasing to cratering instability in polymers under ultrahigh electric fields. *Phys. Rev. Lett.* **106**, 118301. (doi:10.1103/physrevlett.106.118301)

17. Park HS, Wang Q, Zhao X, Klein PA. 2013 Electromechanical instability on dielectric polymer surface: modeling and experiment. *Comput. Methods Appl. Mech. Eng.* **260**, 40–49. (doi:10.1016/j.cma.2013.03.020)
18. Liang X, Cai S. 2015 Shape bifurcation of a spherical dielectric elastomer balloon under the actions of internal pressure and electric voltage. *J. Appl. Mech.-T. ASME* **82**, 101002. (doi:10.1115/1.4030881)
19. Xie Y-X, Liu J-C, Fu YB. 2016 Bifurcation of a dielectric elastomer balloon under pressurized inflation and electric actuation. *J. Mech. Phys. Solids* **78–79**, 182–188. (doi:10.1016/j.jisolsr.2015.08.027)
20. Carpi F, Frediani G, Turco S, De Rossi D. 2011 Bioinspired tunable lens with muscle-like electroactive elastomers. *Adv. Funct. Mater.* **21**, 4152–4158. (doi:10.1002/adfm.201101253)
21. Shian S, Diebold RM, Clarke DR. 2013 Tunable lenses using transparent dielectric elastomer actuators. *Opt. Express* **21**, 8669. (doi:10.1364/oe.21.008669)
22. Son S, Pugal D, Hwang T, Choi HR, Koo JC, Lee Y, Kim K, Nam J-D. 2012 Electromechanically driven variable-focus lens based on transparent dielectric elastomer. *Appl. Opt.* **51**, 2987. (doi:10.1364/ao.51.002987)
23. Ho S, Banerjee H, Foo YY, Godaba H, Aye WMM, Zhu J, Yap CH. 2017 Experimental characterization of a dielectric elastomer fluid pump and optimizing performance via composite materials. *J. Intel. Mat. Syst. Str.* **28**, 3054–3065. (doi:10.1177/1045389×17704921)
24. Li Z, Zhu J, Foo CC, Yap CH. 2017 A robust dual-membrane dielectric elastomer actuator for large volume fluid pumping via snap-through. *Appl. Phys. Lett.* **111**, 212901. (doi:10.1063/1.5005982)
25. Mao G, Wu L, Fu Y, Chen Z, Natani S, Gou Z, Ruan X, Qu S. 2018 Design and characterization of a soft dielectric elastomer peristaltic pump driven by electromechanical load. *IEEE-ASME T. Mech.* **23**, 2132–2143. (doi:10.1109/tmech.2018.2864252)
26. Kaltseis R, Keplinger C, Baumgartner R, Kaltenbrunner M, Li T, Mächler P, Schwödiauer R, Suo Z, Bauer S. 2011 Method for measuring energy generation and efficiency of dielectric elastomer generators. *Appl. Phys. Lett.* **99**, 162904. (doi:10.1063/1.3653239)
27. Li T, Qu S, Yang W. 2012 Energy harvesting of dielectric elastomer generators concerning inhomogeneous fields and viscoelastic deformation. *J. Appl. Phys.* **112**, 34119. (doi:10.1063/1.4745049)
28. Li T, Keplinger C, Baumgartner R, Bauer S, Yang W, Suo Z. 2013 Giant voltage-induced deformation in dielectric elastomers near the verge of snap-through instability. *J. Mech. Phys. Solids* **61**, 611–628. (doi:10.1016/j.jmps.2012.09.006)
29. Wang F, Yuan C, Lu T, Wang TJ. 2017 Anomalous bulging behaviors of a dielectric elastomer balloon under internal pressure and electric actuation. *J. Mech. Phys. Solids* **102**, 1–16. (doi:10.1016/j.jmps.2017.01.021)
30. Liang X, Cai S. 2018 New electromechanical instability modes in dielectric elastomer balloons. *Int. J. Solids Struct.* **132–133**, 96–104. (doi:10.1016/j.jisolsr.2017.09.021)
31. Wang H, Lei M, Cai S. 2013 Viscoelastic deformation of a dielectric elastomer membrane subject to electromechanical loads. *J. Appl. Phys.* **113**, 213508. (doi:10.1063/1.4807911)
32. Zhao X, Koh SJA, Suo Z. 2011 Nonequilibrium thermodynamics of dielectric elastomers. *Int. J. Appl. Mech.* **3**, 203–217. (doi:10.1142/s1758825111000944)
33. Foo CC, Cai S, Koh SJA, Bauer S, Suo Z. 2012 Model of dissipative dielectric elastomers. *J. Appl. Phys.* **111**, 34102. (doi:10.1063/1.3680878)
34. Gent AN. 1996 A new constitutive relation for rubber. *Rubber Chem. Technol.* **69**, 59–61. (doi:10.5254/1.3538357)
35. Zhao X, Hong W, Suo Z. 2007 Electromechanical hysteresis and coexistent states in dielectric elastomers. *Phys. Rev. B* **76**, 134113. (doi:10.1103/physrevb.76.134113)
36. Suo Z. 2010 Theory of dielectric elastomers. *Acta Mech. Solida Sin.* **23**, 549–578. (doi:10.1016/s0894-9166(11)60004-9)
37. Kofod G, Sommer-Larsen P, Kornbluh R, Pelrine R. 2003 Actuation response of polyacrylate dielectric elastomers. *J. Intel. Mat. Syst. Str.* **14**, 787–793. (doi:10.1177/104538903039260)
38. Suo Z, Zhao X, Greene W. 2008 A nonlinear field theory of deformable dielectrics. *J. Mech. Phys. Solids* **56**, 467–486. (doi:10.1016/j.jmps.2007.05.021)
39. Wissler M, Mazza E. 2007 Mechanical behavior of an acrylic elastomer used in dielectric elastomer actuators. *Sensor. Actuat. A-Phys.* **134**, 494–504. (doi:10.1016/j.sna.2006.05.024)

40. Michel S, Zhang XQ, Wissler M, Löwe C, Kovacs G. 2009 A comparison between silicone and acrylic elastomers as dielectric materials in electroactive polymer actuators. *Polym. Int.* **59**, 391–399. (doi:10.1002/pi.2751)
41. Guo J, Xiao R, Park HS, Nguyen TD. 2015 The temperature-dependent viscoelastic behavior of dielectric elastomers. *J. Appl. Mech.-T. ASME* **82**, 091009. (doi:10.1115/140308501)
42. Mao G, Huang X, Diab M, Li T, Qu S, Yang W. 2015 Nucleation and propagation of voltage-driven wrinkles in an inflated dielectric elastomer balloon. *Soft Matter* **11**, 6569–6575. (doi:10.1039/c5sm01102g)